

Refined mean field model of heat and momentum transfer in magnetoconvection

Till Zürner^{a)}

*Institut des Sciences de la Mécanique et Applications Industrielles (IMSIA),
 ENSTA-ParisTech/CNRS/CEA/EDF/Institut Polytechnique de Paris,
 828 Boulevard des Maréchaux, 91120 Palaiseau, France*

(Dated: September 9, 2020)

In this article, the theoretical model on heat and momentum transfer for Rayleigh-Bénard convection in a vertical magnetic field by Zürner *et al.* (Phys. Rev. E **94**, 043108 (2016)) is revisited. Using new data from recent experimental and numerical studies the model is simplified and extended to the full range of Hartmann numbers, reproducing the results of the Grossmann-Lohse theory in the limit of vanishing magnetic fields. The revised model is compared to experimental results in liquid metal magnetoconvection and shows that the heat transport is described satisfactorily. The momentum transport, represented by the Reynolds number, agrees less well which reveals some shortcomings in the theoretical treatment of magnetoconvection.

I. INTRODUCTION

Magnetoconvection considers the interaction of magnetic fields with thermal convection flows in electrically conducting fluids. The most notable examples of such systems in nature are liquid iron cores of planets and the plasma inside stars generating global magnetic fields in the so-called dynamo effect.^{1,2} In technological applications, magnetoconvection may be relevant for liquid metal batteries³ and in proposed liquid metal cooling blankets for fusion reactors.⁴ The study of magnetoconvection is numerically and experimentally difficult due to the extreme conditions that often govern these systems. Additionally, the most relevant fluids are liquid metals and plasmas which are either very hard or impossible to handle experimentally. A theoretical understanding of canonical setups is thus important to understand the relevant mechanisms at play and to predict their behavior beyond the currently accessible parameter space.

In a previous article,⁵ a theoretical model was developed to predict the heat and momentum transfer in a Rayleigh-Bénard convection (RBC) system subject to a vertical magnetic field. It utilized the ansatz by Grossmann and Lohse⁶ and incorporated the effect of Joule dissipation induced by the magnetic field. The preceding works of Chakraborty⁷ on the same topic should be mentioned here as well. At the time, the study suffered the lack of numerical and especially experimental data which limited a proper evaluation and validation of the theory. However, after a number of new studies have been published on the topic over the past few years the model can be revisited and revised. The aim of the present article is (i) to simplify the existing model by reducing its number of free parameters as well as by reconsidering the validity of the included physical

mechanisms and (ii) to extend it to a larger parameter space.

Rayleigh-Bénard convection considers a horizontal fluid layer of height H heated at its lower boundary and cooled at its upper boundary with constant temperatures T_{bot} and T_{top} , respectively, where $T_{\text{top}} < T_{\text{bot}}$. A fluid with a sufficiently large electrical conductivity σ can be influenced by imposing a magnetic field which in the present case is a homogeneous vertical magnetic field $\mathbf{B}_0 = B_0 \mathbf{e}_z$ (with z as vertical axis). The flow is controlled by five dimensionless parameters

$$\begin{aligned} \text{Ra} &= \frac{g\alpha\Delta TH^3}{\nu\kappa}, & \text{Ha} &= B_0 H \sqrt{\frac{\sigma}{\rho_0 \nu}}, \\ \text{Pr} &= \frac{\nu}{\kappa}, & \text{Pm} &= \frac{\nu}{\eta}, & \Gamma &= \frac{L}{H}. \end{aligned} \quad (1)$$

The Rayleigh number Ra quantifies the thermal driving of the fluid by the temperature difference $\Delta T = T_{\text{bot}} - T_{\text{top}}$ and the Hartmann number Ha gives a measure of the magnetic field strength. The fluid is characterized by the thermal Prandtl number Pr and the magnetic Prandtl number Pm which compare the kinematic viscosity ν to the thermal diffusivity κ and the magnetic diffusivity $\eta = 1/(\mu\sigma)$, respectively. Lastly, the aspect ratio Γ is the ratio of horizontal extent L of the fluid layer and the layer height H . The remaining quantities are the acceleration due to gravity g , the magnetic permeability μ , the volumetric thermal expansion coefficient α and the mass density ρ_0 of the fluid at a reference temperature T_0 . An alternative parameter to the Hartmann number is the Chandrasekhar number $Q = \text{Ha}^2$. Of major interest in the convection research are the globally averaged quantities of heat and momentum transport, represented by the Nusselt and Reynolds number

$$\text{Nu} = 1 + \frac{H\langle u_z T \rangle}{\kappa\Delta T}, \quad \text{Re} = \frac{UH}{\nu}, \quad (2)$$

respectively. The symbol $\langle \cdot \rangle$ denotes an average over the fluid volume and time. The characteristic velocity U is the speed

^{a)}Electronic mail: till.zuerner@ensta-paris.fr;
<https://orcid.org/0000-0001-6488-6611>

Table I. Parameters of experimental and numerical data on RBC with a vertical magnetic field in chronological order. Listed are the Prandtl number Pr and the range of Rayleigh and Hartmann numbers ($Ra_{\min/\max}$ and $Ha_{\min/\max}$). Experiments are marked by E and direct numerical simulations by S. In addition, the cell aspect ratio Γ is given as *diameter* : *height* for cylindrical cells and as *width* : *depth* : *height* for rectangular cells. For Cioni, Chaumat, and Sommeria¹⁸, corresponding data at $Ha = 0$ were published in Ref. 10.

	Reference	Pr	Ra_{\min}	Ra_{\max}	Ha_{\min}	Ha_{\max}	Γ
E	Cioni, Chaumat, and Sommeria ¹⁸	0.025	2×10^7	3×10^9	850	1980	1 : 1
E	Aurnou and Olson ¹⁹	0.025	4×10^2	7×10^4	26	35	8.3 : 8.3 : 1
E	Burr and Müller ²⁰	0.020	3×10^3	1×10^5	10	120	10 : 20 : 1
E	King and Aurnou ¹³	0.024	2×10^6	2×10^8	0	1110	1 : 1
S	Liu, Krasnov, and Schumacher ²²	0.025	1×10^7	1×10^7	0	2000	4 : 4 : 1
S	Yan <i>et al.</i> ²³	1	1×10^4	8×10^{10}	0	10 000	periodic
		0.025	2×10^7	1.7×10^8	1414	1414	periodic
S	Lim <i>et al.</i> ²⁴	8	5×10^5	1×10^{10}	0	800	1 : 1 : 1
E	Zürner <i>et al.</i> ²¹	0.029	1×10^6	6×10^7	0	1050	1 : 1
S	Akhmedagaev <i>et al.</i> ²⁵	0.025	1×10^7	1×10^9	0	1400	1 : 1

of the mean wind in the convective flow. It is generally estimated by the root-mean-square (rms) average of the velocity field $\mathbf{v} = v_i \mathbf{e}_i$ over the whole fluid volume $U = \langle v_i^2 \rangle^{1/2}$. Another parameter of the magnetoconvection system is the magnetic Reynolds number $Rm = PmRe$. It compares the advection of the magnetic field by the flow to its diffusion. More detailed, at high $Rm > 1$ the magnetic field can be deformed by the flow, while at low $Rm \ll 1$ alterations to the external field \mathbf{B}_0 can generally be neglected.¹

Experimental investigations of magnetoconvection require a working fluid with a sufficiently large electrical conductivity. In the vast majority of cases, liquid metals are the only option fitting this criterion. Their high electrical conductivity $\sigma \sim 10^6$ S/m also gives them a good thermal conductivity which places them in the low Prandtl number regime $Pr \ll 1$. Experiments with a watery sulfuric acid ($Pr = 12$, $\sigma \sim 10^2$ S/m) do exist,⁸ though to reach the same Ha as in liquid metals magnetic fields of two orders of magnitude higher strength are required. Flow measurements in liquid metals are very difficult due to their opaque nature and high heat fluxes are necessary to reach large Rayleigh numbers compared to other common fluids such as air or water. Notable early works in liquid metal RBC without magnetic field include Ref. 9–12. In recent years the topic experienced a number of new experimental efforts.^{13–17} Experiments of RBC including the effects of a vertical magnetic field are much more rare. When the initial theory⁵ on heat and momentum transport in magnetoconvection was published, only data by Cioni, Chaumat, and Sommeria¹⁸ at high $Ha \geq 850$ and Ra up to 3×10^9 were available. Other studies^{19,20} were at very low $Ra \leq 10^5$ and $Ha \leq 120$. Since then, experimental heat transport data by King and Aurnou¹³ and Zürner *et al.*²¹ were published, the latter including the currently sole measurements of the velocity field in liquid metal RBC with a vertical magnetic field. The parameter ranges covered by the now available experimental data are summarized in Table I.

Numerical simulations of turbulent RBC with a vertical magnetic field at low Prandtl numbers are published by Liu,

Krasnov, and Schumacher²², Yan *et al.*²³ and Akhmedagaev *et al.*²⁵ (all at $Pr = 0.025$). Simulations at higher Pr exist by Yan *et al.*²³ ($Pr = 1$) and Lim *et al.*²⁴ ($Pr = 8$). Their advantage over experiments is, of course, the full knowledge of the convective velocity field. However, for small Pr exhaustive parameter surveys are prohibitively expensive in terms of computation power. Nonetheless, their detailed insights on magnetoconvection are instrumental in revising the theoretical model. The parameters of the above publications are listed in Table I. Some studies focusing on magnetoconvection close to the onset should be mentioned here as well^{26–28}.

This article is structured as follows. The next section II recapitulates the central ideas of the Grossmann-Lohse (GL) approach as the basis of the theoretical model. In section III the different aspects of the magnetoconvection model are reviewed. Where necessary, they are altered or extended. The updated model is evaluated with the available experimental data and its results are discussed in section IV. Lastly, section V gives the final conclusions and a short discussion.

II. THE MAGNETOHYDRODYNAMIC EXTENSION OF THE GROSSMANN-LOHSE MODEL

For completeness, the framework of the theoretical model of heat and momentum transfer in magnetoconvection is outlined here. It is based on Ref. 5 which builds on the original works by Grossmann and Lohse^{6,29–32}, an updated parameter fit by Stevens *et al.*³³ (both for the nonmagnetic convection case; see also Bhattacharya *et al.*³⁴ and Bhattacharya, Verma, and Samtaney³⁵ for a slightly modified approach) and investigations by Chakraborty⁷ for the magnetoconvection case. The GL theory considers the volume- and time-averaged viscous and thermal energy dissipation rates (DR) – ε_v and ε_κ , respectively – in

the convective flow

$$\varepsilon_v = \frac{\nu}{2} \left\langle (\partial_i v_j + \partial_j v_i)^2 \right\rangle, \quad (3a)$$

$$\varepsilon_\kappa = \kappa \left\langle (\partial_i T)^2 \right\rangle, \quad (3b)$$

$$\varepsilon_\eta = \frac{\eta}{2} \left\langle (\partial_i b_j - \partial_j b_i)^2 \right\rangle. \quad (3c)$$

Here, the Einstein summation convention is used over the coordinates $i, j = x, y, z$ and $\partial_i \equiv \partial/\partial x_i$ is a short notation for the spatial partial derivatives. In the case of magnetoconvection, the additional magnetic DR ε_η due to Joule dissipation has to be considered. Since the imposed magnetic field \mathbf{B}_0 is homogeneous, only the secondary magnetic field $\mathbf{b} = b_i \mathbf{e}_i$ induced by the interaction of \mathbf{v} and \mathbf{B}_0 is relevant for the calculation of the magnetic DR. It should be mentioned that the above definition of ε_η differs by a factor of $1/(\mu\rho_0)$ from other studies.^{5,7} This is done to have consistent units for the three dissipation rates: $[\varepsilon_v] = (\text{m/s})^2/\text{s}$, $[\varepsilon_\kappa] = \text{K}^2/\text{s}$ and $[\varepsilon_\eta] = \text{T}^2/\text{s}$ with the above definitions.

The GL approach is a mean field theory since only average quantities are considered. As a result, the aspect ratio Γ or the cell geometry is not incorporated explicitly into the theory and the effect of side walls, which can constrain the transport, is neglected. Only the top and bottom boundaries of the fluid layer are relevant. They are always assumed to be rigid and electrically insulating which results in a no-slip boundary condition for the velocity field.

The averaged DR in (3) are of importance since in statistically stationary turbulence the exact equations

$$\varepsilon_v + \frac{\varepsilon_\eta}{\mu\rho_0} = \frac{\nu^3}{H^4} \frac{(\text{Nu} - 1)\text{Ra}}{\text{Pr}^2}, \quad \varepsilon_\kappa = \kappa \frac{(\Delta T)^2}{H^2} \text{Nu} \quad (4)$$

can be obtained.^{7,36} In the GL theory, the second term on the left-hand-side of the first equation is not present,⁶ since in that case $\varepsilon_\eta = 0$. The GL approach now splits the DR into their contributions from characteristic regions of the flow, namely the bulk and the boundary layer (BL)

$$\varepsilon_v = \varepsilon_{v,\text{Bulk}} + \varepsilon_{v,\text{BL}}, \quad (5a)$$

$$\varepsilon_\eta = \varepsilon_{\eta,\text{Bulk}} + \varepsilon_{\eta,\text{BL}}, \quad (5b)$$

$$\varepsilon_\kappa = \kappa \frac{(\Delta T)^2}{H^2} + \varepsilon_{\kappa,\text{Bulk}} + \varepsilon_{\kappa,\text{BL}}. \quad (5c)$$

The term $\kappa(\Delta T)^2/H^2$ in (5c) is the contribution of pure heat conduction to ε_κ . For high Nusselt numbers this term is often neglected in comparison to the advection based contributions of the bulk and BL regions but becomes relevant in low-Nu regimes.³² Now, the individual contributions in (5) are estimated by considering that the bulk dissipation is dominated by inertia and the BL dissipation by viscous effects. These estimates are then multiplied by free model parameters and combined with (4) and (5) to form the model equations. In the present article, the model fit parameters of the GL theory (i.e., $\text{Ha} = 0$) are referred to by capital letters A and C_1 to C_4 (corresponding to a and c_1 to c_4 in Ref. 33) and the parameters of the present magnetoconvection model are denoted by small letters a and c_1 to c_6 . Note, that the parameters C_i and c_i do

not correspond to the same terms. The initial model⁵ utilized the following estimates for the DR contributions

$$\varepsilon_{v,\text{Bulk}} \sim \frac{U^3}{H} = \frac{\nu^3}{H^4} \text{Re}^3, \quad (6a)$$

$$\varepsilon_{v,\text{BL}} \sim \nu \frac{U^2}{\delta_{v,B}^2} \frac{\delta_{v,B}}{H} = \frac{\nu^3}{H^4} \text{Re}^2 \text{Ha}, \quad (6b)$$

$$\varepsilon_{\eta,\text{Bulk}} \sim \eta \frac{\text{Rm}^2 B_0^2}{H^2} = \mu\rho_0 \frac{\nu^3}{H^4} \text{Re}^2 \text{Ha}^2, \quad (6c)$$

$$\varepsilon_{\eta,\text{BL}} \sim \eta \frac{\text{Rm}^2 B_0^2}{\delta_{v,B}^2} \frac{\delta_{v,B}}{H} = \mu\rho_0 \frac{\nu^3}{H^4} \text{Re}^2 \text{Ha}^3, \quad (6d)$$

$$\varepsilon_{\kappa,\text{Bulk}} \sim \frac{(\Delta T)^2 U}{H} = \kappa \frac{(\Delta T)^2}{H^2} \text{RePr}, \quad (6e)$$

$$\varepsilon_{\kappa,\text{BL}} \sim \kappa \frac{(\Delta T)^2}{H^2} \sqrt{\text{RePr}}. \quad (6f)$$

The above scaling relations are based on the following assumptions (more information on their derivation can be found in Appendix A 1): (i) The Prandtl number is restricted to the $\text{Pr} \ll 1$ case of liquid metals. (ii) The Hartmann number is large enough, that the viscous boundary layers at the top and bottom boundary have to be substituted by Hartmann layers. The viscous BL thickness δ_v transforms then to $\delta_{v,B} = H/\text{Ha}$. For the $\text{Ha} = 0$ case, the GL theory assumes a Blasius-type BL with a thickness $\delta_{v,0} = aH/\sqrt{\text{Re}}$, where a is a free parameter.²⁹ The thermal BL thickness, given by $\delta_T = H/(2\text{Nu})$, is unaffected by this assumption.²⁵ (iii) The magnetic Reynolds number is sufficiently low, $\text{Rm} \ll 1$, so that the quasistatic approximation can be applied. This means that, compared to the external magnetic field \mathbf{B}_0 , the effect of the induced magnetic field \mathbf{b} on the eddy currents can be neglected. Since liquid metals have $\text{Pm} \sim 10^{-6}$, very high Reynolds numbers of $\text{Re} \sim 10^6$ are needed to invalidate this assumption. In this approximation, the magnitude of \mathbf{b} can be estimated as $b \sim \text{Rm}B_0$.¹

Additionally, three regime transitions are introduced to account for changes in the estimates (6) for different parameter regimes (for more details see Appendix A 2). First, the velocity scale within the thermal BL is U if $\delta_T > \delta_v$. However, for the case $\delta_T < \delta_v$ the velocity scale $U\delta_T/\delta_v$ has to be used instead.⁶ This change in scaling is introduced²⁹ by replacing $\text{Re} \rightarrow \text{Re}f(\delta_{v,B}/\delta_T)$ in (6e) and (6f) with the transition function $f(x) = (1 + x^4)^{-1/4}$. Secondly, $\varepsilon_{v,\text{Bulk}} \propto \text{Re}^3$ in (6a) assumes a turbulent flow, while after a transition to a weakly non-linear flow the scaling is better represented by $\varepsilon_{v,\text{Bulk}} \propto \text{Re}^2$. This is facilitated by multiplying $\varepsilon_{v,\text{Bulk}}$ by $g(\text{Re}/\text{Re}^*)$, where $g(x) = f(1/x)^{-1}$ and Re^* is a model parameter characterizing the position of transition to fully turbulent convection.⁵ The last transition concerns the onset of convection, which is not naturally recovered by the model and is imposed by replacing occurrences of $\text{Nu} - 1$ by $(\text{Nu} - 1)/h(\text{Ra}/\text{Ra}_c)$ with the transition function $h(x) = 1 - f(x)$. The critical Rayleigh number Ra_c is calculated in the Chandrasekhar limit³⁷ as $\text{Ra}_c = \pi^2 \text{Ha}^2$ which is valid for $\text{Ha} \gtrsim 100$. This last replacement has to be done only in the model equation used to calculate Nu .⁵

With these considerations implemented, the final model equations are calculated by multiplying the estimates (6a)

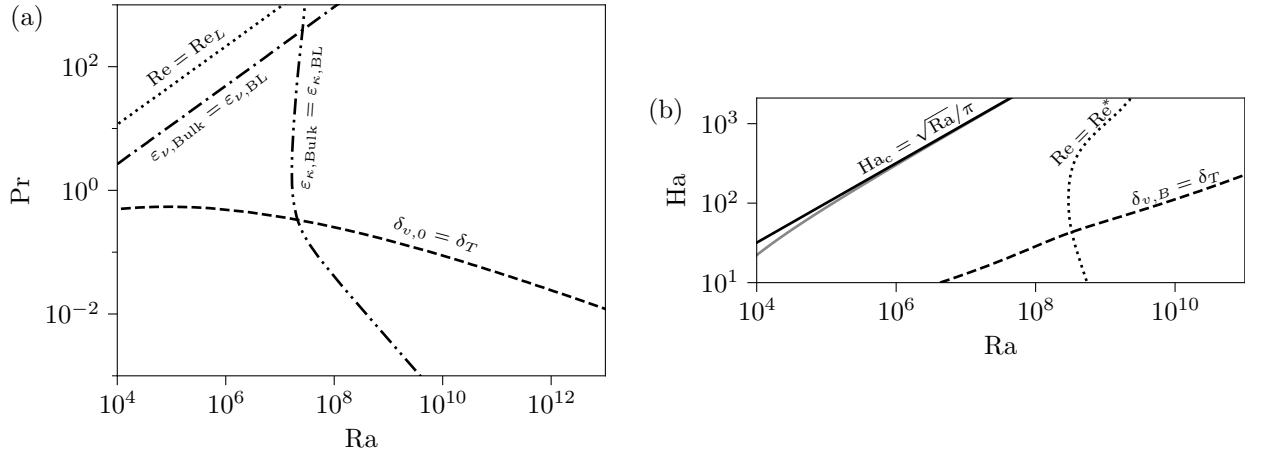


Figure 1. (a) Phase diagram of the GL theory at $Ha = 0$ spanned by Rayleigh number Ra and Prandtl number Pr according to Stevens *et al.*³³ Shown are the transition boundaries for the BL crossover $\delta_{v,0} = \delta_T$ (dashed line), the equivalence of bulk and BL dissipation for the viscous DR $\varepsilon_{v,Bulk} = \varepsilon_{v,BL}$ (dash-dotted line) and thermal DR $\varepsilon_{\kappa,Bulk} = \varepsilon_{\kappa,BL}$ (dash-double-dotted line) and the transition to the large-Pr regime at $Re = Re_L = 3.4$ (dotted line). (b) (Ra, Ha) phase diagram of the initial model for magnetocovection at $Pr = 0.025$ according to Zürner *et al.*⁵ Shown are the transition boundaries for the BL crossover $\delta_{v,B} = \delta_T$ (dashed line), the transition to the fully turbulent regime at $Re = Re^* = 5.6 \times 10^4$ (dotted line) and the Chandrasekhar limit $Ha_c = \sqrt{Ra}/\pi$ (solid line). For comparison, the real solution of Ha_c from a linear stability analysis³⁷ is plotted as a solid gray line.

to (6f) with the free model parameters c_1 to c_6 , respectively, and combining them with (4) and (5). The result is⁵

$$Re = \frac{\left(\sqrt{c_6^2 + 4c_5(Nu - 1)} - c_6\right)^2}{4c_5^2 Pr f(2Nu/Ha)}, \quad (7a)$$

$$\frac{(Nu - 1)Ra}{\mathcal{R}^2 Pr^2 h(Ra/Ra_c)} = c_1 \mathcal{R} g\left(\frac{\mathcal{R}}{Re^*}\right) + c_2 Ha + c_3 Ha^2 + c_4 Ha^3 \quad (7b)$$

$$\text{with } \mathcal{R} = \frac{\left(\sqrt{c_6^2 + 4c_5(Nu - 1)/h(Ra/Ra_c)} - c_6\right)^2}{4c_5^2 Pr f(2Nu/Ha)}.$$

Equation (7b) contains Nu , Ra , Ha and Pr only. If the values of the model parameters c_1 to c_6 and Re^* are known, it can be used to numerically calculate Nu for a point in the (Ra, Ha, Pr) phase space. Once Nu is known, Re can be obtained from (7a).

Since the model parameters c_1 to c_6 and Re^* are *a priori* unknown, they have to be determined by fitting equations (7) to experimental data sets of (Ra, Ha, Pr, Nu) and at least one data point (Ra, Ha, Pr, Nu, Re) including the Reynolds number. In Ref. 5, using the heat transfer data by Cioni, Chaumat, and Sommeria¹⁸ and numerical results for the momentum transport, the parameter values $c_1 = 0.053$, $c_2 = -2.4$, $c_3 = 0.014$, $c_4 = -3.7 \times 10^{-6}$, $c_5 = 0.0038$, $c_6 = 0.47$ and $Re^* = 5.6 \times 10^4$ were obtained. Figure 1 shows the regime diagrams of the GL theory³³ at $Ha = 0$ and of the initial model⁵ at $Pr = 0.025$. These will be used as reference in the following discussion.

III. MODIFICATIONS OF THE FRAMEWORK

The original model can be significantly revised by considering its validity boundaries and which assumptions or mech-

anisms are applicable in that range of parameters. Each of the following sections considers one aspect of the initial model equations (7). Some aspects of the model will be corrected as required and new aspects are introduced.

A. The crossover of the thermal and kinetic BL

The first topic concerns the velocity scale within the thermal BL. As discussed in section II, the characteristic velocity is chosen as U if $\delta_T > \delta_v$ and as $(\delta_T/\delta_v)U$ if $\delta_T < \delta_v$, which is implemented by the transition function $f(\delta_{v,B}/\delta_T)$ in the initial model (7) and by $f(\delta_{v,0}/\delta_T)$ in the GL theory.²⁹ This, however, entails an unnecessary complication of the model for low Pr . Simulations^{38,39} at $Ha = 0$ and $Pr = 0.025$ show that the viscous BL is smaller than the thermal BL $\delta_v < \delta_T$. This is also reflected by the results of the GL theory which gives the BL crossover $\delta_{v,0} = \delta_T$ for $Pr > 0.1$ up to $Ra = 10^{11}$ (Fig. 1(a)). By applying a magnetic field, the kinetic BL is decreased due to its eventual transformation²⁴ into a Hartmann layer $\delta_{v,B} \propto 1/Ha$. Conversely, the thermal boundary layer thickness $\delta_T \propto 1/Nu$ increases since experiments and simulations in low- Pr magnetocovection have shown that Nu generally decrease for increasing Ha .^{13,18,21,22} That means that the presence of the $\delta_{v,B} = \delta_T$ regime boundary in the initial model (see dashed line in Fig. 1(b)) is implausible and a result of the insufficient coverage of the low- Ha regime by the experimental data used for fitting the model parameters. The discrepancy between the model and experimental data is shown in Fig. 2. Measured Nusselt numbers taken from Zürner *et al.*²¹ (symbols) are compared to the predictions of the initial model (7) (lines) at three selected Ra . For high $Ha > 200$, the model captures the experimental results well, but deviates from the experiments at small Ha . Especially for $Ha \rightarrow 0$,

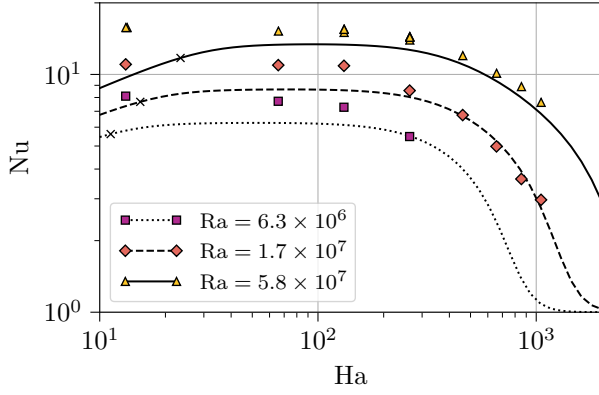


Figure 2. Comparison of experimental Nusselt number data²¹ (filled markers) with the predictions of the initial model⁵ (lines) at $\text{Pr} = 0.029$ for selected Ra . The position of the BL crossover $\delta_{v,B} = \delta_T$ is marked by crosses on the respective lines.

the experimental Nu data saturate at a constant value while the model predictions start to decrease. This coincides with the boundary layer crossover $\delta_{v,B} = \delta_T$ which is marked by a cross on each line. These considerations show that the BL crossover is not relevant for small Pr and can actually result in wrong predictions for the low- Ha regime. It will thus be eliminated from the revised model equations, i.e., the transition function f is removed.

The BL crossover only becomes relevant at moderate or high Pr . Simulations of magnetoconvection²⁴ at $\text{Pr} = 8$ found a BL crossover with $\delta_v > \delta_T$ below an optimal Hartmann number. It is also of interest that the crossover is tied to a short increase of the Nusselt number compared to its value at $\text{Ha} = 0$. As seen in Fig. 2, the transition function f emulates such a behavior by generating a local maximum of Nu . That means, if the present model was to be extended to the intermediate and high Pr case the transition function f may be of importance and could be reintroduced. However, this is not part of the scope of the present work.

B. The limit of small Hartmann numbers

In the model equations (7), the Hartmann BL $\delta_{v,B} = H/\text{Ha}$ is used to characterize the kinetic BL. This is not applicable for the limit $\text{Ha} \rightarrow 0$, where the kinetic BL is better described by a Prandtl-Blasius type BL $\delta_{v,0} = aH/\sqrt{\text{Re}}$ as used by the GL theory.⁶ Lim *et al.*²⁴ proposed a general BL thickness δ_v based on a dimensional analysis that connects these two types of BL

$$\delta_v = \left(\delta_{v,0}^{-2} + \delta_{v,B}^{-2} \right)^{-1/2} = \frac{H}{\sqrt{\text{Re} a^{-2} + \text{Ha}^2}}. \quad (8)$$

For high $\text{Ha} \rightarrow \infty$, (8) becomes a Hartmann layer $\delta_v \rightarrow \delta_{v,B}$ and at vanishing magnetic fields the Prandtl-Blasius BL is recovered $\delta_v \rightarrow \delta_{v,0}$. Replacing $\delta_{v,B}$ with δ_v in the BL

contribution of the kinetic and magnetic DR in (6b) and (6d) results in the modified estimates

$$\varepsilon_{v,\text{BL}} \sim \frac{\nu^3}{H^4} \sqrt{\text{Re}^5 a^{-2} + \text{Re}^4 \text{Ha}^2}, \quad (9a)$$

$$\varepsilon_{\eta,\text{BL}} \sim \mu \rho_0 \frac{\nu^3}{H^4} \sqrt{\text{Re}^5 \text{Ha}^4 a^{-2} + \text{Re}^4 \text{Ha}^6}. \quad (9b)$$

In the high Ha limit, these estimates recover the initial scalings (6). For $\text{Ha} \rightarrow 0$, $\varepsilon_{\eta,\text{BL}}$ vanishes and $\varepsilon_{v,\text{BL}}$ becomes the estimate of the GL theory⁶ $\varepsilon_{v,\text{BL}} \sim (\nu^3/H^4)\text{Re}^{5/2}$.

C. Transition towards laminar bulk flow and onset of convection

The GL ansatz⁶ assumes the existence of a turbulent large-scale wind of velocity U in the convection cell. Even with the subsequent extension towards a laminar high- Pr case²⁹, the scaling of the viscous bulk DR has always been assumed to be dominated by inertia ($\varepsilon_{v,\text{Bulk}} \propto \text{Re}^3$). The initial model for magnetoconvection⁵ introduced a transition between the turbulent Re^3 -scaling towards a laminar Re^2 -scaling of $\varepsilon_{v,\text{Bulk}}$ at a characteristic Reynolds number of Re^* which was evaluated to $\text{Re}^* = 5.6 \times 10^4$. The phase diagram in Fig. 1(b) shows this transition to happen at $\text{Ra} > 10^8$ for all Ha . However, especially for the $\text{Ha} = 0$ case it is well-known that turbulence in low- Pr convection sets in at much smaller Rayleigh numbers.^{40–42} Since the bulk turbulence is a central assumption of the model, it is evident that this scaling transition on its own is insufficient to model the weakly non-linear and laminar regimes at high Ha . The transition function g and the model parameter Re^* are consequently removed from the model equations.

The onset of convection cannot be recovered intrinsically by the current model and would require a proper treatment of the non-turbulent regimes with a complete overhaul of the model ansatz. This, however, is beyond the scope of this study. The transition towards the purely conductive regime was previously imposed at the Chandrasekhar limit by a fixed transition function h in Ref. 5. This approach will be retained and the results of the revised model with and without the imposed onset transition are compared in section IV.

The critical Rayleigh number in the Chandrasekhar limit $\text{Ra}_c = \pi^2 \text{Ha}^2$ is valid only for $\text{Ha} \gtrsim 100$. To allow for the limit $\text{Ha} \rightarrow 0$ discussed in the previous section, the argument of the onset transition function h is replaced based on the critical Hartmann number: $h(\text{Ha}_c^2/\text{Ha}^2)$. In the Chandrasekhar limit, $\text{Ha}_c = \sqrt{\text{Ra}}/\pi$ which is valid for $\text{Ra} \gtrsim 2 \times 10^5$ and all Ha with a deviation of $\leq 10\%$ from the proper solution obtained by a linear stability analysis.³⁷ Since $\text{Ha}_c^2/\text{Ha}^2 = \text{Ra}/\text{Ra}_c$ in the Chandrasekhar limit, this change has only an effect on the validity boundaries of the model.

Recently, simulations²² and experiments²¹ proved the existence of convective flows for $\text{Ha} > \text{Ha}_c$ concentrated near the lateral walls of the convection cell. They are denoted as wall modes that cannot be included in the present mean-field theory which neglects the effect of side-walls.

D. Revised model equations

The initial and new DR contribution estimates (6) and (9) are multiplied by the model parameters c_1 to c_6 and combined with equations (4) and (5)

$$\frac{(\text{Nu} - 1)\text{Ra}}{\text{Pr}^2} = c_1 \text{Re}^3 + c_2 \sqrt{\text{Re}^5 a^{-2} + \text{Re}^4 \text{Ha}^2} + c_3 \text{Re}^2 \text{Ha}^2 + c_4 \sqrt{\text{Re}^5 \text{Ha}^4 a^{-2} + \text{Re}^4 \text{Ha}^6}, \quad (10)$$

$$\text{Nu} - 1 = c_5 \text{RePr} + c_6 \sqrt{\text{RePr}}. \quad (11)$$

For the case $\text{Ha} = 0$, the second model equation (11) does not change while equation (10) becomes

$$\frac{(\text{Nu} - 1)\text{Ra}}{\text{Pr}^2} = c_1 \text{Re}^3 + \frac{c_2}{a} \text{Re}^{5/2}. \quad (12)$$

(12) and (11) are equal to the GL model equations³³ for the low-Pr regime, i.e., if the regime transitions for the BL crossing and for the high-Pr limit are removed. Consequently, the parameters in (12) and (11) can be identified with the values of the GL theory³³

$$\begin{aligned} a &= A = 0.922, \\ c_1 &= C_2 = 1.38, \quad c_2 = AC_1 = 7.42, \\ c_5 &= C_4 = 0.0252, \quad c_6 = C_3 = 0.487, \end{aligned} \quad (13)$$

with $C_1 = 8.05$. The only remaining unknown parameters are thus c_3 and c_4 . This is a significant reduction of the number of free parameters compared to the seven fit coefficients of the initial model. The two remaining parameters need to be fitted to experimental data (see section IV). The original fit⁵ resulted

$$\begin{aligned} \frac{(\text{Nu} - 1)\text{Ra}}{h(\text{Ha}_c^2/\text{Ha}^2)\text{Pr}^2} &= C_2 \mathcal{R}^3 + AC_1 \sqrt{\mathcal{R}^5 A^{-2} + \mathcal{R}^4 \text{Ha}^2} + c_3 \mathcal{R}^2 \text{Ha}^2 + c_4 \sqrt{\mathcal{R}^5 \text{Ha}^4 A^{-2} + \mathcal{R}^4 \text{Ha}^6}, \\ \text{with } \mathcal{R} &= \frac{\left(\sqrt{C_3^2 + 4C_4(\text{Nu} - 1)/h(\text{Ha}_c^2/\text{Ha}^2)} - C_3 \right)^2}{4C_4^2 \text{Pr}}. \end{aligned} \quad (14)$$

Once the values of c_3 and c_4 are determined, (14) can be numerically solved for Nu with a given set of $(\text{Ra}, \text{Ha}, \text{Pr})$. The corresponding Reynolds number then follows from (11)

$$\text{Re} = \frac{\left(\sqrt{C_3^2 + 4C_4(\text{Nu} - 1)/h(\text{Ha}_c^2/\text{Ha}^2)} - C_3 \right)^2}{4C_4^2 \text{Pr}}. \quad (15)$$

IV. RESULTS

The model equation (14) is fitted to the experimental data sets $(\text{Ra}, \text{Ha}, \text{Pr}, \text{Nu})$ by Cioni, Chaumat, and Sommeria¹⁸,

in some negative parameter values. Since only positive coefficients are physically sensible for dissipation rates, the bounds $(0, \infty)$ are imposed on the two parameters during the fitting process.

The initial model for magnetoconvection as well as the GL theory suffer from an ambiguity, where the magnitude of the Reynolds number cannot be determined by heat transport data $(\text{Ra}, \text{Ha}, \text{Pr}, \text{Nu})$ alone: Re can be re-scaled by an arbitrary constant factor without affecting the predicted value of the Nusselt number (see Appendix B for more details). As a result, at least one full data-set $(\text{Ra}, \text{Ha}, \text{Pr}, \text{Nu}, \text{Re})$ is required to fix the magnitude of Re . By identifying the parameters a , c_1 , c_2 , c_5 and c_6 with the coefficients of the original GL theory in (13), this ambiguity has already been resolved for the revised model. The implications of this choice of parameters on the Reynolds number are discussed in section IV A by comparing it to experimental data.

To fit the model equations to data sets of $(\text{Ra}, \text{Ha}, \text{Pr}, \text{Nu})$, the Reynolds number is eliminated from (10) using (11). To impose the onset of convection, $\text{Nu} - 1$ is replaced⁵ by $(\text{Nu} - 1)/h(\text{Ha}_c^2/\text{Ha}^2)$ where $h(x) = 1 - (1 + x^4)^{-1/4}$

King and Aurnou¹³ and Zürner *et al.*¹⁷ The data by Aurnou and Olson¹⁹ and Burr and Müller²⁰ are not used, since they have no data $\text{Ra} > 2 \times 10^5$ which is required by the Chandrasekhar limit approximation (section III C). The resulting parameter values of the model including the onset of convection are

$$c_3 = 0.0449, \quad c_4 = 7.52 \times 10^{-18} \approx 0. \quad (16)$$

The fit returns a standard deviation of 0.0044 for c_3 , i.e., a relative uncertainty of 10%. This is a large improvement compared to the initial model, in which the parameter had relative uncertainties of $\sim 100\%$ due to the lack of data.⁵ The c_4 parameter has a fit standard deviation of 2.74×10^{-6} . Compared with its nominal value in (16), c_4 can thus be treated

as zero, i.e., $\varepsilon_{\eta, \text{BL}}$ has no influence on the result. This means either that the effect of Joule dissipation in the viscous BL is negligible or that it is only relevant at high magnetic fields $\text{Ha} > 2000$, beyond the currently available experiments (see Table I). The latter could be the case, since $\varepsilon_{\eta, \text{BL}} \propto \text{Ha}^3$ may increase significantly for high Ha .

If the onset of convection is excluded (i.e., $h(\text{Ha}_c^2/\text{Ha}^2) \equiv 1$), the fitted parameter values become $c_3 = 0.0520 \pm 0.0058$ and $c_4 = 5.19 \times 10^{-19} \pm 3.66 \times 10^{-6} \approx 0$. The difference between the model predictions with and without imposed onset is investigated in the following section IV A (see also Figs. 4 and 5(b)).

Lifting the fitting boundaries of $(0, \infty)$ results in a small negative fit value of $c_4 = (-9.56 \pm 0.26) \times 10^{-5}$ and $c_3 = 0.0599 \pm 0.0044$. The negative parameter causes the numerical solution of the model to become unstable for intermediate Ha . For example, in the phase space covered by the experimental data the predictions of Nu and Re at $\text{Ha} \sim 1000$ can reach magnitudes of 10 times their value at $\text{Ha} = 0$. The model only produces sensible results in the low- and high- Ha regime, where the c_4 -term in (14) has no influence (as the term vanishes for $\text{Ha} \rightarrow 0$ and the model is dominated by the imposed transition function h for large Ha). This reinforces the choice to explicitly restrict c_3 and c_4 to positive values and that c_4 vanishes.

A. Comparison with experimental data

Figure 3 compares the Nusselt number calculated from the model equation (14) with the experimental data (filled markers) used for fitting the parameters c_3 and c_4 . Plotted are the theoretical predictions of the revised model including the onset of convection (black lines) and of the initial model⁵ (gray lines).

The data by Zürner *et al.*²¹ in Fig. 3(a) are well reproduced by the revised model. It correctly reproduces the saturation of Nu for low $\text{Ha} \rightarrow 0$ while the initial model declines as discussed previously in Fig. 2. Close to the onset of convection both models give similar predictions as the onset transition function h dominates the results. In this range of high Ha , the revised model slightly underpredicts the experimental data.

Nusselt number data by Cioni, Chaumat, and Sommeria¹⁸ (Fig. 3(c)) also fit well with the theoretical results. Here, the revised model generally overpredicts the experimental data near the onset of convection. The exact progression of Nu with increasing Ra is not exactly the same, with the revised model approaching a straight line (i.e., a power law) while the experiment is showing a curvature, but the general trend and magnitude are recovered. The initial model reproduces the slope of the experimental data better for the highest Ra . This is not surprising since these were the only data used to fit the parameter of the initial model in Ref. 5. Then again, this better agreement does not extend to low Ra near the onset of convection where the initial model has even higher values than the revised model.

The data by King and Aurnou¹³ (Fig. 3(b)) agree less well with the revised model which approaches the data with in-

creasing Ra , but consistently underpredicts the experiments. Especially for $\text{Ha} = 994$, the onset of convection at the Chandrasekhar limit (at $\text{Ra}_c = 9.7 \times 10^6$, marked by an open circle) is not visible in the experiment. This is in stark contrast to the other experiments (e.g. the $\text{Ha} = 850$ data in Fig. 3(c)). The initial model produces very similar results except for the lowest $\text{Ha} = 98$, where its predictions are even lower than the revised model. This deviation for low Ha is in agreement with the previously discussed data in Fig. 3(a).

Figure 4 replots the experimental data (filled markers) and the revised model with imposed onset (black lines) from Fig. 3 but compares them to the revised model without the imposed onset of convection (gray lines). The two revised models are identical for low Ha (Fig. 4(a)) and show only slight differences for large Ra (Fig. 4(b) and (c)). However, close to the Chandrasekhar limit they deviate strongly from one another. This shows that the model is not intrinsically applicable outside the regime of turbulent convection and why the Chandrasekhar limit is imposed explicitly using a transition function.

Experimental data for the Reynolds number are available from the experiments by Zürner *et al.*²¹ The velocity field is probed using ten ultrasound Doppler velocimetry (UDV) sensors and a characteristic global velocity scale is determined by calculating the rms-average of the measured velocities over time and over all sensors. The resulting global Reynolds number $\text{Re}_{\text{global}}$ is compared to the theoretical predictions in Fig. 5. In the low- Ha limit, the revised model with onset (black lines) correctly reproduces the saturation of Re at a constant value. This saturation value is the same as the measured values of $\text{Re}_{\text{global}}$, though this should be interpreted as purely coincidental. As shown in Ref. 17, the GL theory underpredicts Reynolds numbers based on the turbulent large-scale wind in low- Pr convection by nearly a factor of two. Due to the choice (13) of model parameters, this discrepancy is also present in the revised model for magnetoconvection. At the same time, the magnitude of $\text{Re}_{\text{global}}$ is affected by many low-velocity areas of the flow that lie within the measurement volume of the UDV sensors. Coincidentally, this also reduces its magnitude by a factor of about two compared to a wind-based Reynolds number.²¹ Nonetheless, the agreement between $\text{Re}_{\text{global}}$ and the theoretical predictions for small Ha shows, that the scaling of the Reynolds number is correctly recovered for $\text{Ha} \rightarrow 0$ while its magnitude only deviates by a constant factor at these Pr . It is possible to re-scale the theoretical Reynolds number to match the wind-based Reynolds number from experiments at low Pr . The effects of such a modification are discussed in Appendix B.

By comparing Figs. 3(a) and 5(a), it can be seen that the Reynolds number measurements start to decrease from their value at $\text{Ha} = 0$ at lower Ha than the Nusselt number²¹, i.e., they have a shorter saturation plateau. Since in the model equation (15) Re is directly linked to Nu , the revised model does not recover this behavior and the predicted Re stays constant up to the same value of Ha where Nu starts to drop off. Also, the onset transition function forces Re to drop off very fast when approaching the Chandrasekhar limit while $\text{Re}_{\text{global}}$ decreases at a much slower rate due to the presence of wall modes past the Chandrasekhar limit.^{21,22} The main issue is that in mag-

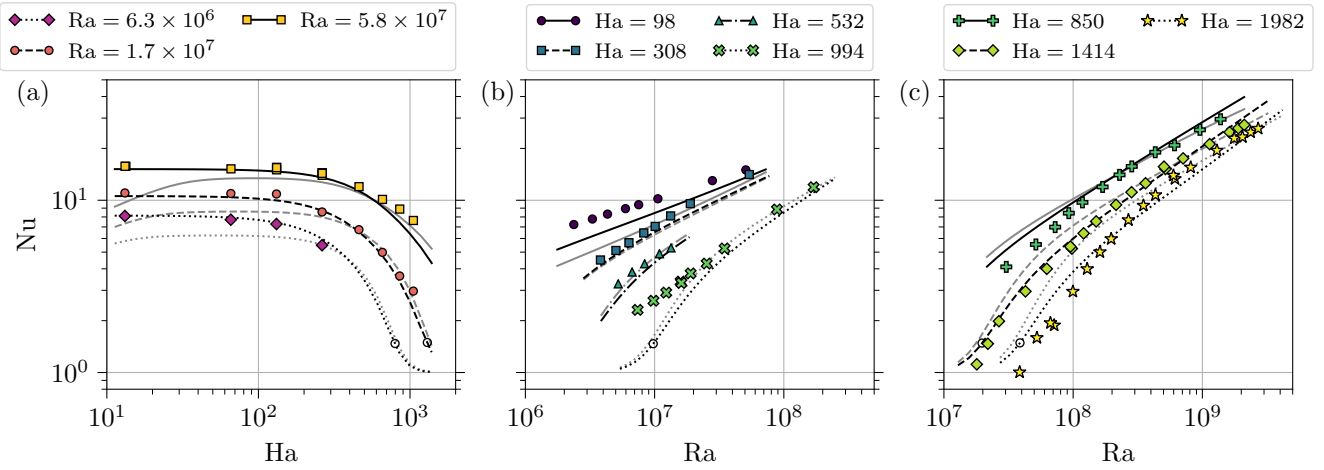


Figure 3. Comparison of Nusselt number data from experiments (filled markers) with theoretical predictions (lines). Gray lines are the result of the initial model⁵ and black lines are the revised model with imposed onset of convection. The position of the Chandrasekhar limit is indicated by an open circle on the respective black line. The experimental data are selected from the data sets used for the fitting of the model: (a) Zürner *et al.*²¹ (Nu vs. Ha at selected Ra and Pr = 0.029), (b) King and Aurnou¹³ (Nu vs. Ra at selected Ha and Pr = 0.024), (c) Cioni, Chaumat, and Sommeria¹⁸ (Nu vs. Ra at selected Ha and Pr = 0.025). The gray lines and markers in (a) are identical to the lines and markers in Fig. 2.

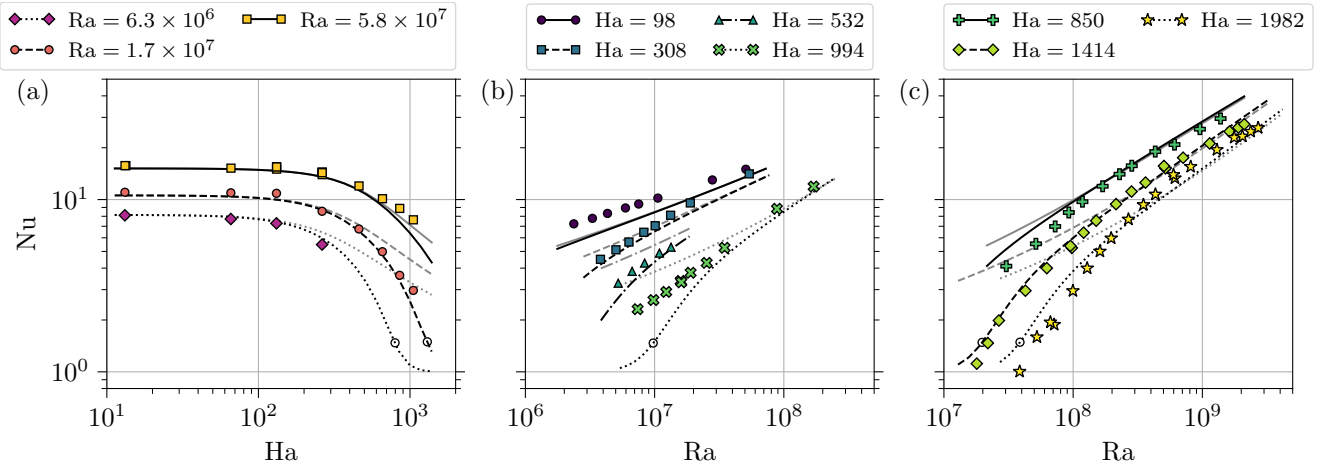


Figure 4. Comparison of Nusselt number predictions of the revised model with (black lines) and without (gray lines) imposed onset of convection. The position of the Chandrasekhar limit is indicated by an open circle on the respective black line. The experimental data (filled markers) and black lines are identical to Fig. 3. (a) Nu vs. Ha at selected Ra and Pr = 0.029 with measurements by Zürner *et al.*²¹ (b) Nu vs. Ra at selected Ha and Pr = 0.024 with measurements by King and Aurnou¹³ (c) Nu vs. Ra at selected Ha and Pr = 0.025 with measurements by Cioni, Chaumat, and Sommeria.¹⁸

netoconvection the degree of turbulence in the flow is not directly linked to the magnitude of the average velocity magnitude. A combination of high Ra and high Ha might produce the same Reynolds number of the large scale flow as another combination of low Ra and low Ha, but with weaker turbulent fluctuations.²¹ This disconnects the progression of Re from that of Nu, the latter being dependent on the mean velocity magnitude as well as velocity fluctuations.²⁴ This effect is not included in the model equations and as a result, the model does not recover the progression of the Reynolds number correctly, except for the low-Ha limit.

However, even with these discrepancies the revised model represents an improvement over the results of the initial model

(gray lines in Fig. 5(a)). The initial model was fitted using numerical Reynolds number data⁵ based on the rms-velocity over the whole fluid volume. As discussed before, it is expected that the resulting predictions are approximately twice as high as the Re_{global} data. This is only true for the largest measured $Ra > 10^7$, whereas for lower Ra the initial model can even underpredict the measurements. Additionally, the initial Re predictions starts to decrease for $Ha \rightarrow 0$ instead of saturating at a constant value, albeit not as prominently as for Nu (Fig. 3(a)). Close to the Chandrasekhar limit, the initial and the revised model converge to the same solution due to the effect of the imposed onset transition function.

The revised model without imposed onset of convection is

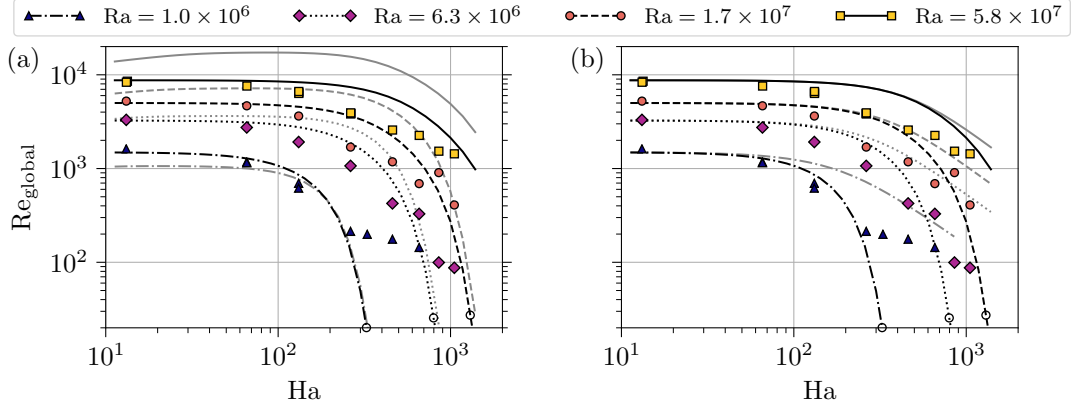


Figure 5. Comparison of Reynolds number data from experiments (filled markers) with theoretical predictions (lines). Shown is Re vs. Ha at selected Ra and $Pr = 0.029$ with measurements by Zürner *et al.*²¹ (Re_{global} is based on a rms-average over all velocity data measured in the experiment). The experimental data correspond to the Nusselt number measurements shown in Figs. 3(a) and 4(a). The black lines show the results of the revised model with imposed onset of convection. The position of the Chandrasekhar limit is indicated by an open circle on the respective black line. The gray lines are the results of (a) the initial model⁵ and (b) the revised model without the imposed onset of convection. Filled markers and black lines are identical in panels (a) and (b).

shown in Fig. 5(b) as gray lines. Like for the case of Nu (Fig. 4(a)), Re drops off much more slowly for increasing Ha than with an imposed transition function. One could observe that the slope of the lines past the Chandrasekhar limit are similar to the decrease of the experimental data, albeit at a higher magnitude. However, since these data are dominated by wall modes which the model cannot take into account, this similarity should be seen as coincidental.

In conclusion, the revised model represents an improvement over the initial model for nearly the whole range of Ra and Ha . Especially the extension into the low- Ha limit has been implemented successfully for both Re and Nu . In light of the discrepancies between the experimental data (e.g. compare $Ha = 994$ and 850 in Figs. 3(b) and (c)), the revised model manages to create a satisfactory reproduction of the Nusselt number for all experimental data sets. In contrast, the Reynolds number predictions do not agree as well with the experimental data. This points to some mechanisms in magnetoconvection (e.g. the suppression of turbulence) that are not yet properly treated in the model. Lastly, the necessity to impose the onset of convection through a transition function highlights that the weakly non-linear and laminar regimes need to be addressed separately to intrinsically reproduce the Chandrasekhar limit.

B. Regime diagram and validity boundaries

Figure 6(a) shows the phase diagram of the revised model at $Ha = 0$ (black lines) in comparison to the GL theory (gray lines). The BL crossover ($\delta_v = \delta_T$, dashed line) is positioned at only slightly smaller Pr than the result of the GL theory. Below this line ($\delta_v < \delta_T$), the regime boundaries of the thermal DR contribution crossover ($\mathcal{E}_{K,\text{Bulk}} = \mathcal{E}_{K,\text{BL}}$, dash-double-dotted line) coincide for the revised model and the GL theory. This is expected since the model recovers the GL model equations in the low- Pr limit. For Pr above the BL crossover ($\delta_v > \delta_T$), this

regime boundary and the kinetic DR contribution crossover ($\mathcal{E}_{v,\text{Bulk}} = \mathcal{E}_{v,\text{BL}}$, dash-dotted line) deviate strongly from one another, indicating that the model is not applicable for these regimes.

The validity of the model is limited by the following assumptions. (i) The working fluid has a low Prandtl number $Pr \ll 1$. This implies that $\delta_v < \delta_T$ and the BL crossover is thus considered as regime boundary for the low- Pr regime. (ii) The Chandrasekhar limit is assumed for the critical Hartmann number $Ha_c = \sqrt{Ra}/\pi$ which is valid for $Ra > 2 \times 10^5$. (iii) The quasistatic approximation applies, i.e., $Rm \ll 1$. For a typical magnetic Prandtl number for liquid metals of $Pm \sim 10^{-6}$, this implies that a Reynolds number of $Re \sim 10^6$ has to be reached to violate this assumption. The gray shaded area in Fig. 6(a) shows the validity range of the revised model defined by the above boundaries (i) to (iii). For decreasing and increasing Ra , the limiting boundaries are $Ra = 2 \times 10^5$ and $Re = 10^6$ (dotted line), respectively. With increasing Pr , the model reaches up to the $\delta_v = \delta_T$ boundary (dashed line).

Turning to the case $Ha > 0$, Figs. 6(b) and (c) show the (Ra, Ha) phase diagrams for the characteristic Prandtl numbers $Pr = 0.025$ (mercury, gallium) and $Pr = 0.005$ (sodium), respectively. Displayed are the same regime boundaries as in Fig. 6(a) together with the Chandrasekhar limit (solid black line). Since the revised model is applicable for all Hartmann numbers, there are no vertical boundaries to the validity range (gray shaded areas). For low Ra , the model is, again, limited by $Ra = 2 \times 10^5$. For high Ra and $Pr = 0.025$, the validity boundaries are the BL crossover at low $Ha \lesssim 10^3$ and the $Re = 10^6$ boundary for higher Ha . At $Pr = 0.005$, the BL crossover is shifted to very high $Ra > 10^{13}$ (see also Fig. 6(a)) and the $Re = 10^6$ boundary is the limiting restriction for increasing Ra at all Ha . Since the validity of the quasistatic approximation is dependent on the magnetic Prandtl number, these limits may shift for increasing or decreasing Pm (the boundary is shifted to smaller or higher Ra , respectively).

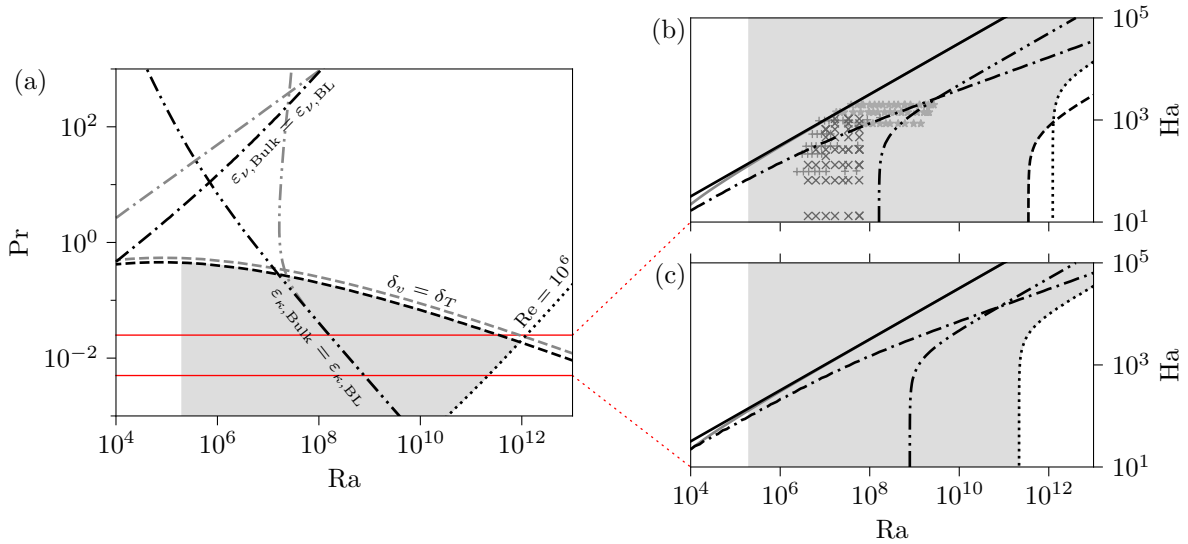


Figure 6. Regime diagram and validity boundaries (gray shaded areas) of the revised magnetoconvection model including the onset of convection. (a) (Ra, Pr) phase diagram for $Ha = 0$. Shown are the transition boundaries for the BL crossover $\delta_v = \delta_T$ (dashed line), $Re = 10^6$ (dotted line) and the equivalence of bulk and BL dissipation for the viscous DR $\varepsilon_{v,Bulk} = \varepsilon_{v,BL}$ (dash-dotted line) and thermal DR $\varepsilon_{\kappa,Bulk} = \varepsilon_{\kappa,BL}$ (dash-double-dotted line). The corresponding regime boundaries of the GL theory³³ are re-plotted as gray lines from Fig. 1(a). (b) and (c) (Ra, Ha) phase diagram for $Pr = 0.025$ (mercury, gallium) and $Pr = 0.005$ (sodium), respectively. These Prandtl numbers are marked in (a) by horizontal lines. The critical Hartmann number Ha_c is displayed in the Chandrasekhar limit (solid black line) and as the rigorous linear stability solution (gray solid line). The remaining lines correspond to the regime boundaries in (a). The gray markers in (b) indicate the experiments used to fit the revised model: Cioni, Chaumat, and Sommeria¹⁸ (stars), King and Aurnou¹³ (pluses) and Zürner *et al.*²¹ (crosses). They mark the region of support for the parameter fit – all other areas are extrapolated by the model from this region.

The DR contribution crossovers for the kinetic and thermal DR are also plotted in Figs. 6(b) and (c) (dash-dotted and dash-double-dotted lines, respectively). $\varepsilon_{v,Bulk}$ is dominant at low Ha but is eventually surpassed by $\varepsilon_{v,BL}$ when Ha increases. The thermal DR is generally more dependent on Ra with $\varepsilon_{\kappa,BL}$ and $\varepsilon_{\kappa,Bulk}$ being dominant at low and high Ra , respectively. With decreasing Pr , the kinetic DR crossovers is shifted to higher Ha . The thermal DR crossover at low Ha shifts to higher Ra for decreasing Pr . At high Ha , however, it is unaffected by changes in Pr and runs parallel to the Chandrasekhar limit. Since the parameter c_4 is extremely small, the magnetic DR is dominated by $\varepsilon_{\eta,Bulk}$ for all Ra and Ha .

In summary, the comparison with experimental data (Figs. 3 to 5) and the phase diagrams (Fig. 6) show that despite the reduced complexity of the revised model, its predictions are more accurate and more physically sensible compared to the previous model in Ref. 5.

V. CONCLUSION

An updated model of the heat and momentum transport for Rayleigh-Bénard convection in a vertical magnetic field was presented. By revising some of the basic assumptions of the model and including new aspects, the theoretical predictions could be improved significantly. The inclusion of a generalized kinetic boundary layer thickness allowed for the extension of the model to the low- Ha limit and to match it with the well established Grossmann-Lohse theory at $Ha = 0$. This reduced the complexity of the model greatly by fixing the values of

five parameters. With the removal of the turbulent-to-laminar transition, the total number of free model parameters has thus been reduced from the initial seven to just two. An extended experimental database also allowed for a more robust fit of the model which effectively removed one more parameter ($c_4 \approx 0$). Physically, this suggests that the effect of Joule dissipation in the kinetic boundary layer is negligible for the considered parameter range. The transitions of the boundary layer crossover and the high Prandtl number limit from the Grossmann-Lohse theory are excluded in the present low- Pr regime. If the model were to be extended to higher Prandtl numbers, these transitions could be easily reintroduced. In this case it might also be beneficial to consider a modification of the Grossmann-Lohse ansatz presented by Bhattacharya, Verma, and Samtaney³⁵ (for $Ha = 0$), who let the model parameters c_i be functions of Ra and Pr . This change can produce more accurate predictions especially of the Reynolds number over a wider range of Pr .

The revised model equations satisfactorily reproduce experimental heat transport data for liquid metals at $Pr \sim 0.025$. Additional experimental data at different Prandtl numbers, for example in liquid sodium with $Pr \sim 0.005$, would be desirable to further verification of the model. The momentum transport predictions agree less well with experimental results. This shows that the suppression of turbulence by the magnetic field cannot be fully reproduced by the Grossmann-Lohse ansatz. Together with a more rigorous treatment of the weakly non-linear and laminar regimes this is a major challenge for this mean-field theory and should be considered in future investigations.

ACKNOWLEDGMENTS

The author would like to thank Jörg Schumacher for insightful discussions and helpful suggestions. This work was supported by the Deutsche Forschungsgemeinschaft with grant no. GRK 1567.

Appendix A: The model equations

This appendix discusses some details of the model equations that were skipped in the main text for the sake of brevity.

1. The initial dissipation rate estimates

The scaling relations of the dissipation rate (DR) contributions in (6) are based on the following arguments, which were introduced in Ref. 5, 6, and 29.

In the kinetic boundary layer (BL), the velocity gradient is estimated as U/δ_v , using the velocity U of the turbulent large scale wind and the kinetic BL thickness δ_v as characteristic scales. With the definition of the viscous DR (3a), the BL contribution amounts to $\varepsilon_{v,BL} \sim \nu(U/\delta_v)^2$. An additional factor is introduced as the volume fraction of the top and bottom BL compared to the whole fluid volume, which amounts to $2\delta_v/H$ (the constant factor of 2 is dropped in the scaling relation). With an Hartmann layer for the kinetic BL $\delta_v = \delta_{v,B}$, these considerations amount to (6b). The bulk flow is assumed to be dominated by turbulence and that the dissipation term $\nu \nabla^2 \mathbf{v}$ is balanced by the inertial term $(\nabla \cdot \mathbf{v})\mathbf{v}$ through an energy cascade. Using the layer height H and wind velocity U as scales, this gives $\nu U/H^2 \sim U^2/H$ and with the definition (3a) results in (6a). The bulk volume fraction is approximated as $(H - 2\delta_v)/H \sim 1$ for thin BL $\delta_v \ll H$.

The estimates of the magnetic DR (6c,6d) are calculated using its definition (3c). As mentioned in point (iii) after equation (6), the induced magnetic field strength is estimated as $b \sim RmB_0$ and the length scales are the layer height H and the viscous BL thickness δ_v in bulk and BL, respectively. The volume fractions are applied as before for the viscous DR.

The thermal BL contribution follows from the definition (3b), the linearized temperature gradient $\sim \Delta T/\delta_T$ and the BL volume fraction δ_T/H : $\varepsilon_{\kappa,BL} \sim \kappa(\Delta T/\delta_T)^2 \delta_T/H = \kappa(\Delta T/H)^2 Nu$. If this estimate was used, the first term $\kappa(\Delta T/H)^2$ in (5c) would not be required. However, Grossmann and Lohse²⁹ further modified this estimate by balancing the advective term $\mathbf{v} \cdot \nabla T$ of the heat transfer equation in the bulk and the dissipative term $\kappa \nabla^2 T$ in the BL: $U/H \sim \kappa/\delta_T^2$ which gives $Nu \sim \sqrt{RePr}$ and results in the BL contribution estimate (6f). The bulk thermal DR (6e) is determined in direct analogue to the bulk viscous DR. The bulk volume fraction is again estimated as $(H - 2\delta_T)/H \sim 1$ with the thermal BL thickness δ_T .

It has to be noted that the approximation of the thermal bulk volume fraction $(H - 2\delta_T)/H \sim 1$ is not valid close to the onset of convection, where $\delta_T = H/(2Nu) \rightarrow H/2$ since

$Nu \rightarrow 1$. However, with an imposed onset of convection (see black lines Figs. 4 and 5(b)), this region of the phase space is dominated by the transition function h and the bulk volume fraction has little influence on the result. Without an imposed onset of convection (gray lines), the model fails to correctly reproduce the weakly non-linear and laminar regimes which is not changed by including the bulk volume fraction in the model equations. Additionally, explicit inclusion of the bulk volume fraction would make equation (11) incompatible with the corresponding GL model equation³³ and the direct association of parameters (13) between the models for $Ha = 0$ would be impeded. As a consequence, the estimate (6e) is left unchanged.

2. Regime transitions of the initial model

The transition function $f(x) = (1 + x^4)^{-1/4}$ (introduced in Ref. 29) has the properties $f(x \rightarrow 0) \rightarrow 1$ and $f(x \rightarrow \infty) \rightarrow 1/x$. The term $Uf(\delta_{v,B}/\delta_T) = Uf(2Nu/Ha)$ consequently describes the velocity scale in the thermal boundary layer (BL): If the viscous BL is nested within the thermal BL ($\delta_T > \delta_{v,B}$) the outer layers of the thermal BL experience the large-scale wind U and $Uf(\delta_{v,B}/\delta_T \rightarrow 0) \approx U$. Conversely, for $\delta_T < \delta_{v,B}$ the velocity scale in the thermal BL is reduced. Assuming a linear velocity profile in the kinetic BL, this gives a characteristic velocity of $Uf(\delta_{v,B}/\delta_T \rightarrow \infty) \approx U\delta_T/\delta_{v,B}$. The estimates (6e) and (6f) for the initial model thus become $\varepsilon_{\kappa,Bulk} \sim \kappa(\Delta T/H)^2 RePr f(2Nu/Ha)$ and $\varepsilon_{\kappa,BL} \sim \kappa(\Delta T/H)^2 \sqrt{RePr f(2Nu/Ha)}$.

Similarly, $g(x) = f(1/x)^{-1}$ has the properties $g(x \rightarrow 0) \rightarrow 1/x$ and $g(x \rightarrow \infty) \rightarrow 1$. In the initial model⁵, this allowed $\varepsilon_{v,Bulk}$ to transition between a turbulent Re^3 -scaling ($Re \gg Re^*$) and a laminar Re^2 -scaling ($Re \ll Re^*$) at a model parameter Re^* : $\varepsilon_{v,Bulk} \sim (\nu^3/H^4) Re^3 g(Re/Re^*)$.

The third transition function $h(x) = 1 - f(x)$ has the properties $h(x \rightarrow 0) \rightarrow 0$ and $h(x \rightarrow \infty) \rightarrow 1 - 1/x \rightarrow 1$ and is used to enforce the onset of convection⁵. It is expected that $Nu \rightarrow 1$ below the critical Rayleigh number $Ra < Ra_c$, i.e., in the purely conductive regime. Let us assume a solution Nu to a model equation has been found that does not reproduce this behavior (this corresponds to (7b) without h). The onset can be imposed by calculating a new result Nu' with $Nu' - 1 = (Nu - 1)h(Ra/Ra_c)$. To obtain Nu' directly from the model, this equation can be inserted into the model equation. Specifically, every occurrence of $Nu - 1$ is replaced by $(Nu' - 1)/h(Ra/Ra_c)$ (the prime of Nu' is subsequently dropped). The argument of the transition function $f(2Nu/Ha)$ is not modified, since h is only relevant for Ra close to or below Ra_c in which case Nu is small, Ha is large and $f(2Nu/Ha) \approx 1 = \text{const.}$ h is not introduced into the model equation for Re , since $Re \rightarrow 0$ follows intrinsically from (7a) for $Nu \rightarrow 1$.

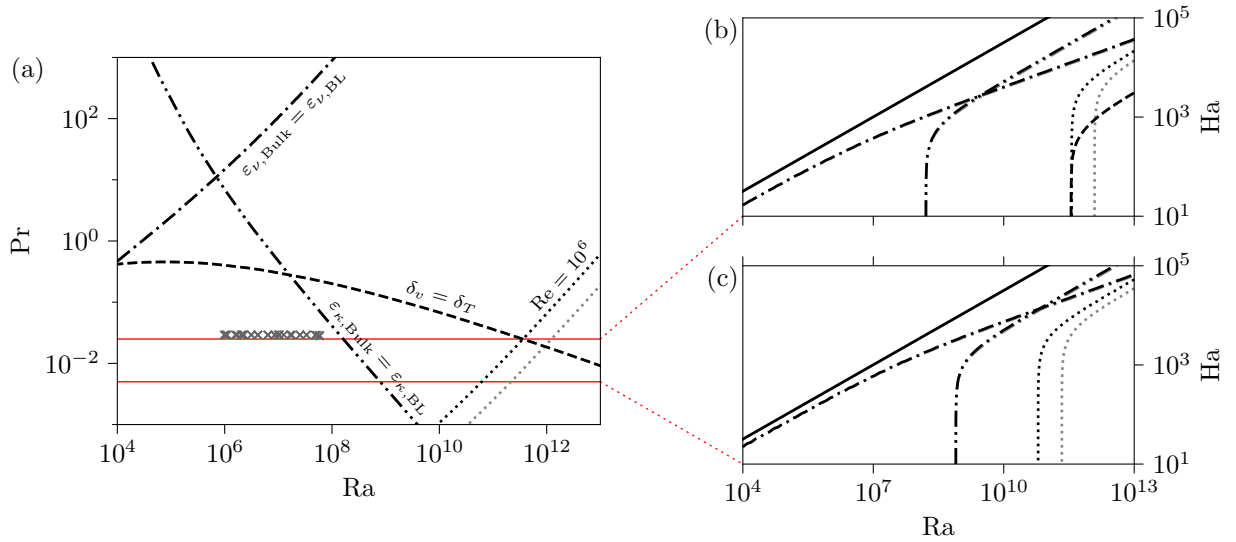


Figure 7. Phase diagrams of the model with onset transition and re-scaled parameters (B3). Regime boundaries are plotted as black lines with the same line styles as in Fig. 6. The corresponding regime boundaries with the un-scaled parameters (13) and (16) are replotted from Fig. 6 as gray lines. (a) (Ra, Pr) phase diagram at Ha = 0. (b) and (c) (Ra, Ha) phase diagram at Pr = 0.025 and Pr = 0.005, respectively. The gray crosses in (a) mark the positions of the Re_{LSC} measurements¹⁷ used to determine β with (B2).

Appendix B: Reynolds number re-scaling

The model equations (10) and (11) are invariant under the transformations

$$\begin{aligned} \text{Re} &\rightarrow \beta \text{Re}, & a &\rightarrow \beta^{1/2} a, \\ c_1 &\rightarrow \beta^{-3} c_1, & c_2 &\rightarrow \beta^{-2} c_2, & c_3 &\rightarrow \beta^{-2} c_3, \\ c_4 &\rightarrow \beta^{-2} c_4, & c_5 &\rightarrow \beta^{-1} c_5, & c_6 &\rightarrow \beta^{-1/2} c_6 \end{aligned} \quad (\text{B1})$$

for any $\beta \in \mathbb{R}$. This means that the Reynolds number can be re-scaled by an arbitrary factor without affecting the result of the Nusselt number. Fitting the model equations (10) and (11) to heat transfer data (Ra, Ha, Pr, Nu) can thus result in an infinite number of fit values a and c_1 to c_6 that are consistent with the transformations (B1), give exactly the same result for Nu, but result in wildly different Reynolds numbers for a given point (Ra, Ha, Pr). Note, that the shape of the function $\text{Re}(\text{Ra}, \text{Ha}, \text{Pr})$ over the phase-space is the same for all these fit results and is just shifted by a constant factor.

In Ref. 17 it was shown, that the Reynolds number of the GL theory underpredicts the experimental Reynolds number Re_{LSC} based on the velocity of the large-scale circulation (LSC), i.e., the convective wind. To adapt Re of the model to the experimental data, the factor β is determined by

$$\beta = \frac{\text{Re}_{\text{LSC}}}{\text{Re}(\text{Ra}, \text{Ha}, \text{Pr})}, \quad (\text{B2})$$

where Re is calculated with model parameters (13) and (16) at the point (Ra, Ha, Pr) at which Re_{LSC} was measured (Ha = 0 and Pr = 0.029 for all measurements in Ref. 17). The average result is $\beta = 1.81 \pm 0.08$ and the resulting re-scaled model

parameters are

$$\begin{aligned} c_1 &= 0.233, & c_2 &= 2.26, & c_3 &= 0.0137, \\ c_4 &= 2.30 \times 10^{-18}, & c_5 &= 0.0139, & c_6 &= 0.362, \\ a &= 1.24. \end{aligned} \quad (\text{B3})$$

Propagation of the standard deviations from β , c_3 and c_4 results in uncertainties of 0.031 for c_1 , 0.20 for c_2 , 0.0018 for c_3 , 8.36×10^{-7} for c_4 , 0.0006 for c_5 , 0.008 for c_6 and 0.03 for a .

While the Nusselt number is unchanged, this scaling of Re has to be considered for the regime boundaries. Figure 7 shows the regime boundaries of the re-scaled model (black lines) in comparison to the un-scaled model (gray lines, replot of the black lines in Fig. 6). The BL crossover and DR contribution crossovers are unchanged, as they are invariant under the transformations (B1) as well. However, the $\text{Re} = 10^6$ boundary is shifted to smaller Ra. As a result, for Pr = 0.025 (Fig. 7(b)) the BL crossover and $\text{Re} = 10^6$ coincidentally take place at the same Ra for Ha $\lesssim 10^2$.

The Reynolds number are adjusted by a constant factor only, since the GL ansatz assumes that all dependencies on the control parameters are covered by the base equations (4) and the dissipation rate estimates including transition functions. Thus, the re-scaled parameters (B3) are only valid for small Prandtl numbers. To get correct results for low-, intermediate- and high-Pr regimes, the GL theory would need to be revisited and revised to properly reproduce all these cases. A possible solution for this issue is presented by Bhattacharya, Verma, and Samtaney³⁵, who modified the GL approach by introducing non-constant parameters $c_i(\text{Ra}, \text{Pr})$ for the case Ha = 0. This alternative approach produced Reynolds number predictions that coincided better with numerical and experimental data over a large range of Pr.

REFERENCES

- ¹P. A. Davidson, *An Introduction to Magnetohydrodynamics*, Cambridge Texts in Applied Mathematics, Vol. 25 (Cambridge University Press, Cambridge, United Kingdom, 2001).
- ²H. K. Moffatt and E. Dormy, *Self-Exciting Fluid Dynamos*, Cambridge Texts in Applied Mathematics, Vol. 59 (Cambridge University Press, Cambridge, 2019).
- ³D. H. Kelley and T. Weier, “Fluid Mechanics of Liquid Metal Batteries,” *Appl. Mech. Rev.* **70**, 020801 (2018).
- ⁴T. Ihli, T. K. Basu, L. M. Giancarli, S. Konishi, S. Malang, F. Najmabadi, S. Nishio, A. R. Raffray, C. V. S. Rao, A. Sagara, and Y. Wu, “Review of blanket designs for advanced fusion reactors,” *Fusion Eng. Des.* **83**, 912–919 (2008).
- ⁵T. Zürner, W. Liu, D. Krasnov, and J. Schumacher, “Heat and momentum transfer for magnetoconvection in a vertical external magnetic field,” *Phys. Rev. E* **94**, 043108 (2016).
- ⁶S. Grossmann and D. Lohse, “Scaling in thermal convection: A unifying theory,” *J. Fluid Mech.* **407**, 27–56 (2000).
- ⁷S. Chakraborty, “On scaling laws in turbulent magnetohydrodynamic Rayleigh-Bénard convection,” *Physica D* **237**, 3233–3236 (2008).
- ⁸K. Aujogue, A. Pothérat, I. Bates, F. Debray, and B. Sreenivasan, “Little Earth Experiment: An instrument to model planetary cores,” *Rev. Sci. Instrum.* **87**, 084502 (2016).
- ⁹T. Takeshita, T. Segawa, J. A. Glazier, and M. Sano, “Thermal turbulence in mercury,” *Phys. Rev. Lett.* **76**, 1465 (1996).
- ¹⁰S. Cioni, S. Ciliberto, and J. Sommeria, “Strongly turbulent Rayleigh-Bénard convection in mercury: Comparison with results at moderate Prandtl number,” *J. Fluid Mech.* **335**, 111–140 (1997).
- ¹¹J. A. Glazier, T. Segawa, A. Naert, and M. Sano, “Evidence against ‘ultrahard’ thermal turbulence at very high Rayleigh numbers,” *Nature* **398**, 307–310 (1999).
- ¹²Y. Tsuji, T. Mizuno, T. Mashiko, and M. Sano, “Mean wind in convective turbulence of mercury,” *Phys. Rev. Lett.* **94**, 034501 (2005).
- ¹³E. M. King and J. M. Aurnou, “Magnetostrophic balance as the optimal state for turbulent magnetoconvection,” *Proc. Natl. Acad. Sci. USA* **112**, 990–994 (2015).
- ¹⁴R. Khalilov, I. Kolesnichenko, A. Pavlinov, A. Mamykin, A. Shestakov, and P. Frick, “Thermal convection of liquid sodium in inclined cylinders,” *Phys. Rev. Fluids* **3**, 043503 (2018).
- ¹⁵T. Vogt, S. Horn, A. M. Grannan, and J. M. Aurnou, “Jump rope vortex in liquid metal convection,” *Proc. Natl. Acad. Sci. USA* **115**, 12674–12679 (2018).
- ¹⁶M. Akashi, T. Yanagisawa, Y. Tasaka, T. Vogt, Y. Murai, and S. Eckert, “Transition from convection rolls to large-scale cellular structures in turbulent Rayleigh-Bénard convection in a liquid metal layer,” *Phys. Rev. Fluids* **4**, 033501 (2019).
- ¹⁷T. Zürner, F. Schindler, T. Vogt, S. Eckert, and J. Schumacher, “Combined measurement of velocity and temperature in liquid metal convection,” *J. Fluid Mech.* **876**, 1108–1128 (2019).
- ¹⁸S. Cioni, S. Chaumat, and J. Sommeria, “Effect of a vertical magnetic field on turbulent Rayleigh-Bénard convection,” *Phys. Rev. E* **62**, R4520–R4523 (2000).
- ¹⁹J. M. Aurnou and P. L. Olson, “Experiments on Rayleigh-Bénard convection, magnetoconvection and rotating magnetoconvection in liquid gallium,” *J. Fluid Mech.* **430**, 283–307 (2001).
- ²⁰U. Burr and U. Müller, “Rayleigh-Bénard convection in liquid metal layers under the influence of a vertical magnetic field,” *Phys. Fluids* **13**, 3247–3257 (2001).
- ²¹T. Zürner, F. Schindler, T. Vogt, S. Eckert, and J. Schumacher, “Flow regimes of Rayleigh-Bénard convection in a vertical magnetic field,” *J. Fluid Mech.* **894**, A21 (2020).
- ²²W. Liu, D. Krasnov, and J. Schumacher, “Wall modes in magnetoconvection at high Hartmann numbers,” *J. Fluid Mech.* **849**, R2 (2018).
- ²³M. Yan, M. A. Calkins, S. Maffei, K. Julien, S. M. Tobias, and P. Marti, “Heat transfer and flow regimes in quasi-static magnetoconvection with a vertical magnetic field,” *J. Fluid Mech.* **877**, 1186–1206 (2019).
- ²⁴Z. L. Lim, K. L. Chong, G.-Y. Ding, and K.-Q. Xia, “Quasistatic magnetoconvection: Heat transport enhancement and boundary layer crossing,” *J. Fluid Mech.* **870**, 519–542 (2019).
- ²⁵R. Akhmedagaev, O. Zikanov, D. Krasnov, and J. Schumacher, “Turbulent convection in strong vertical magnetic field,” *J. Fluid Mech.* **895**, R4 (2020).
- ²⁶A. Basak and K. Kumar, “A model for Rayleigh-Bénard magnetoconvection,” *Eur. Phys. J. B* **88**, 1–10 (2015).
- ²⁷Y. Rameshwar, M. A. Rawoof Sayeed, H. P. Rani, and D. Laroze, “Finite amplitude cellular convection under the influence of a vertical magnetic field,” *Int. J. Heat Mass Transf.* **114**, 559–577 (2017).
- ²⁸H. Mondal, A. Das, and K. Kumar, “Onset of oscillatory Rayleigh-Bénard magnetoconvection with rigid horizontal boundaries,” *Phys. Plasmas* **25**, 012119 (2018).
- ²⁹S. Grossmann and D. Lohse, “Thermal convection for large Prandtl numbers,” *Phys. Rev. Lett.* **86**, 3316–3319 (2001).
- ³⁰S. Grossmann and D. Lohse, “Prandtl and Rayleigh number dependence of the Reynolds number in turbulent thermal convection,” *Phys. Rev. E* **66**, 016305 (2002).
- ³¹S. Grossmann and D. Lohse, “Fluctuations in turbulent Rayleigh-Bénard convection: The role of plumes,” *Phys. Fluids* **16**, 4462–4472 (2004).
- ³²S. Grossmann and D. Lohse, “Thermal convection in small Prandtl number liquids: Strong but ineffective,” *AIP Conf. Proc.* **1076**, 68–75 (2008).
- ³³R. J. A. M. Stevens, E. P. van der Poel, S. Grossmann, and D. Lohse, “The unifying theory of scaling in thermal convection: The updated prefactors,” *J. Fluid Mech.* **730**, 295–308 (2013).
- ³⁴S. Bhattacharya, A. Pandey, A. Kumar, and M. K. Verma, “Complexity of viscous dissipation in turbulent thermal convection,” *Phys. Fluids* **30**, 031702 (2018).
- ³⁵S. Bhattacharya, M. K. Verma, and R. Samtaney, “Forecasting Reynolds and Nusselt numbers in turbulent thermal convection using modified Grossmann-Lohse model,” *arXiv:2007.09583 [physics]* (2020).
- ³⁶B. I. Shraiman and E. D. Siggia, “Heat transport in high-Rayleigh-number convection,” *Phys. Rev. A* **42**, 3650–3653 (1990).
- ³⁷S. Chandrasekhar, *Hydrodynamic and Hydromagnetic Stability*, 3rd ed. (Dover Publications, Inc., New York, 1961).
- ³⁸J. D. Scheel and J. Schumacher, “Global and local statistics in turbulent convection at low Prandtl numbers,” *J. Fluid Mech.* **802**, 147–173 (2016).
- ³⁹J. D. Scheel and J. Schumacher, “Predicting transition ranges to fully turbulent viscous boundary layers in low Prandtl number convection flows,” *Phys. Rev. Fluids* **2**, 123501 (2017).
- ⁴⁰F. H. Busse, “Non-linear properties of thermal convection,” *Rep. Prog. Phys.* **41**, 1929–1967 (1978).
- ⁴¹M. Breuer, S. Wessling, J. Schmalzl, and U. Hansen, “Effect of inertia in Rayleigh-Bénard convection,” *Phys. Rev. E* **69**, 026302 (2004).
- ⁴²J. Schumacher, P. Götzfried, and J. D. Scheel, “Enhanced enstrophy generation for turbulent convection in low-Prandtl-number fluids,” *Proc. Natl. Acad. Sci. USA* **112**, 9530–9535 (2015).